Thermochimica Acta, 95 (1985) 159–178
Elsevier Science Publishers B.V., Amsterdam – Printed in The Netherlands

EFFECT OF THERMAL TREATMENT ON THE STRUCTURE AND TEXTURE OF DIFFERENTLY IMPREGNATED NiO/SiO_2 CATALYSTS

SAID HANAFI, ANWAR AMIN *, SARA M. SOLIMAN ** and SUZY A. SELIM ***
Chemistry Department, Faculty of Science, Ain Shams University, Cairo (Egypt)

(Received 16 May 1985)

ABSTRACT

NiO/SiO_2 catalysts were prepared with Ni contents ranging from 2–15% using a microporous silica support at pH ~11.5. The role of the method of preparation on the resulting catalyst is also investigated. Structural and textural changes were followed using X-ray diffraction, TG and DTA techniques—the surface area measurements were carried out on the parent catalysts and those produced in the temperature range 250–1000°C.

Impregnation of the silica gel in the nickel ammine complex solution (catalyst series 1N–4N) with subsequent drying at 80°C overnight produced crystalline catalysts with two distinct peaks at *d*-spacings of 2.035 and 2.349 Å resulting from a surface silicate. This is easily destroyed by thermal treatment at 250°C for Ni contents $\leqslant$10% but is stable to this temperature for the higher Ni content. Drying the catalyst at room temperature ($3N_b$) gives rise to an amorphous product. A non-crystalline catalyst is also obtained when concentrated ammonia solution is added to the adsorbed nickel salt ($3N_c$). At high Ni content, the hydroxo ligand becomes significant and results in a surface compound in which one silanol group is attacked. This gives rise to a crystalline product at 500°C with characteristic *d*-spacings at 2.201 and 2.049 Å which, subsequently, produces a poorly crystalline NiO product at 1000°C. The presence of this hydroxo ligand is manifested by a small endotherm at 260°C.

At Ni contents below 15% but greater than 2% a small exotherm is observed at ~500°C resulting from a reduction process. Entrained SO_4^{2-} ions present as an impurity are evolved at temperatures > 750°C and can be estimated by TG analysis.

The specific surface area decreases with Ni contents $\leqslant$ 5% but increases for higher Ni contents. Catalyst samples containing 15% Ni possess the highest specific area at all temperatures.

Pore structure analysis showed that microporosity increased with increase in Ni content for the catalyst series 1N–4N. Samples from preparations $3N_b$ and $3N_c$ showed more mesoporosity than that of 3N. Thermal treatment causes widening of the pores for catalysts 1N–3N becoming predominantly mesoporous, co-existing with some micropores. Catalyst samples with 15% Ni remained predominantly microporous–mesoporosity increasing only at 1000°C.

* Faculty of Education, Ain Shams University.
** Egyptian Petroleum Research Institute, Nasr City, Cairo, Egypt.
*** To whom correspondence should be addressed.

0040-6031/85/$03.30

INTRODUCTION

Nickel (II) oxide is a good oxidation catalyst, and, since the source of this activity is considered to be the lattice oxygen exchange, it provides no double-bonded oxygen and thus it oxidizes hydrocarbons completely [1]. Also, reduced NiO supported catalysts are widely used in the hydrogenation reactions, e.g., the selective hydrogenation of steam-cracking of gasoline [2]. The activity of both the unreduced and reduced catalysts is largely dependent on the method of preparation [2–5] of the oxide itself or of the active Ni species on the surface. The mode of distribution of active species along the internal and external surface is a function of the impregnation conditions [4]. The introduction of metal complexes on to silica surfaces to produce more active catalysts has been carried out by several investigators [6–8].

The activity of catalysts is believed, by some authors [9–11], to arise from a minimum size of ordered crystalline structure and from dislocation density and, by others, to arise from other disordered parameters [12,13]. All these factors depend on the initial preparative methods and subsequent thermal treatment. The effect of the support during sintering is also significant [11].

As the porous texture of catalyst particles may greatly modify the kinetics of a catalytic reaction, a textural description of the catalyst is essential. Several authors [14–16] have characterized different NiO/SiO_2 catalysts by various techniques, but the approach to the oxide preparation was mainly through the use of simple salts and a hydroxide or carbonate [3].

A detailed thermal, structural and textural study of a NiO/SiO_2 catalyst prepared from a nickel ammine complex is the aim of the present investigation. Techniques such as DTA, TG and XRD for thermal and structural studies and N_2 adsorption for textural determinations are employed.

EXPERIMENTAL

Materials

Coarse silica gel (B.D.H.) previously characterized to be predominantly microporous [17] was used as a support for nickel oxide.

A series of samples (1N–4N) was prepared by soaking 50 g silica into the solution of nickel ammine complex of the required concentration. The latter was prepared by dissolving the calculated weight of $NiSO_4 \cdot 6H_2O$ in 100 ml water and adding concentrated NH_4OH solution with continuous stirring until the precipitate disappeared, i.e., the nickel was in the ammine complex form. Each admixture was then allowed to stand for 15 days at room temperature, the pH being in the range 11–12, then filtered and washed with distilled water until the filtrate was colourless. The catalyst samples were then dried at 80°C overnight.

To study the effect of preparation method on the resulting catalyst a sample was prepared in a manner similar to that for 3N but without washing, and dried at room temperature—this is denoted by $3N_b$. Also, a sample $3N_c$ was prepared by soaking the silica in 100 ml of nickel sulphate solution of the same concentration as that used for preparing sample 3N. Then, the equivalent amount of ammonium hydroxide required for the formation of the complex was added. The sample was then washed and dried at 80°C overnight. The pH after impregnation was in the range 10–11 for these two samples.

Dehydration products were obtained by heating in the presence of air for 2 h over the temperature range 250–1000°C. Henceforth, the temperature will always follow the sample label in specifying a certain product.

Methods

The nickel content was estimated through the analysis of the impregnating solution before and after soaking of the silica gel using EDTA titrant.

The Ni content estimated as NiO for the various catalyst samples is given in Table 1, column 2.

The X-ray diffraction patterns were obtained by a Philips diffractometer unit, Model PM 9920/03 using Fe-filtered Co-radiation. The *d*-distances were calculated and their relative intensities compared with data in the A.S.T.M. cards [18,19].

Thermogravimetric analysis was carried out in static air using a Stanton-Redcroft thermobalance, type 750/770, the heating rate being 10°C min^{-1}.

Differential thermal analysis curves were recorded by a Netzsch Geratebau GmbH, Selb, apparatus (type No. 348 472C) at a heating rate of 10°C min^{-1}. The inert reference used was α-alumina.

Adsorption–desorption isotherms of nitrogen at 77 K were determined by conventional volumetric gas adsorption.

TABLE 1

Chemical and thermogravimetric analysis data for the investigated catalyst samples

Catalyst sample	Ni content (% NiO)	Wt. loss of initial step (%)	Wt. loss of intermediate step (%)	Sulphate content final step "SO_3" (%)	% SO_4	Total weight loss (%)
1N	2.40	6.3	2.9	0.8	0.96	10.0
2N	4.88	7.6	3.0	0.7	0.84	11.3
3N	9.12	8.8	3.1	1.3	1.56	13.2
4N	15.80	11.7	4.3	1.9	2.35	17.9
$3N_b$	9.12	12.6	1.5	1.6	1.92	15.7
$3N_c$	10.49	9.4	3.2	1.3	1.56	13.9

RESULTS AND DISCUSSION

Structural changes

The X-ray diffraction patterns determined for samples 1N–4N are similar and exhibit two distinct bands at *d*-distances of 2.035 and 2.349 Å, the former being more intense (Fig. 1). A few other peaks of much lower intensity also appear at *d*-distances of 1.434, 1.222 and 1.169 Å. The intensity of the peaks increases only slightly with increase in the Ni content. Samples $3N_b$ and $3N_c$ are completely amorphous. Thus, soaking in Ni ammine complex solution for a long period followed by drying at 80°C seems necessary to obtain a crystalline product, and the duration of soaking alone (15 days) is not the sole criterion [20] for producing this crystallinity.

These two bands together do not characterize a known compound of a Ni silicate species, an oxide or hydroxide [18,19]. By analogy with previous observations [20], the nickel ions, upon attacking the surface, interact, first forming small nuclei which later grow in size (> 50 Å), and drying at such low temperatures as 80°C seems to facilitate the orientation of the surface compound formed.

The peak at 2.035 ($2\theta = 52.2°$) is characteristic for a nickel silicide, a compound which could not possibly exist under our experimental conditions. The band at a *d*-distance of 2.349 Å, though close to 2.392 Å characteristic for NiOOH, yet no other bands characterising this compound appear in our patterns. Besides, the bands of lower intensities are close to those of a Ni_2SiO_4 prepared under high pressure [18,19].

From these criteria it is reasonable to assume that the silica surface is

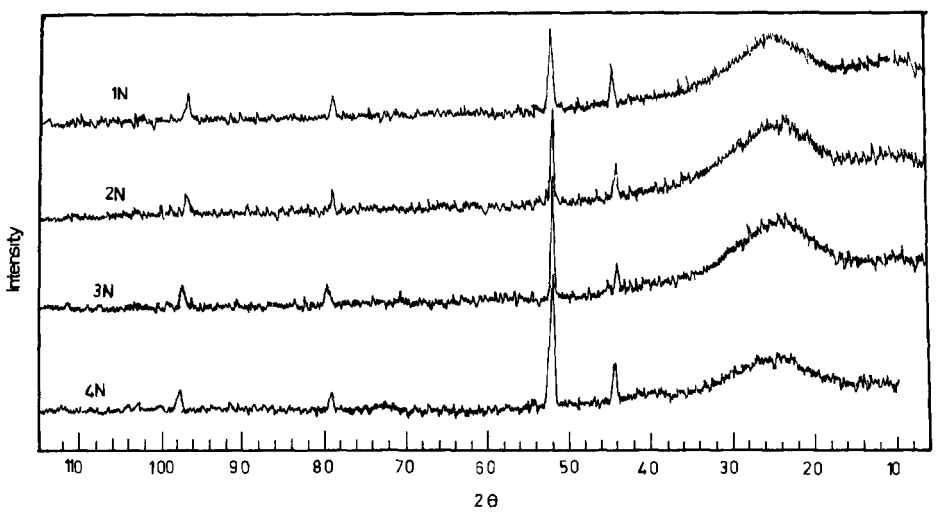

Fig. 1. X-ray diffraction patterns for catalyst series 1N–4N.

polarized [21] at such high pH values. The Ni ammine complex, with ammonia as coordinated ligand, i.e., $[Ni(NH_3)_6]^{2+}$, attacks the silica surface according to the suggested scheme

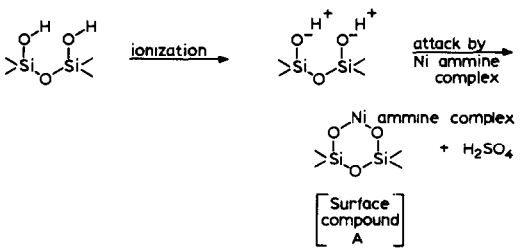

In this case the attack of the ammine complex appears to require the existence of two adjacent hydroxyl groups on the silica surface, with the ammonia ligand being conveniently situated above the Ni ions with an orientation free from steric effects.

It is of significance to note that catalyst 4N was greenish in colour whereas the rest of the samples had an increasing bluish tinge upon decreasing the Ni content. This greenish colouration indicates the presence of an aquo or hydroxo ligand, viz. $[Ni(NH_3)_5OH^-]^+$. The presence of this hydroxo ligand was manifested by the appearance of a small band of the O–H stretching vibration at 3770 cm^{-1} in the IR spectra of sample 4N and, to a lesser extent for sample 3N, and disappeared for the rest of the samples (Fig. 2). In this case, such a Ni hydroxo ammine complex, being monovalent, will

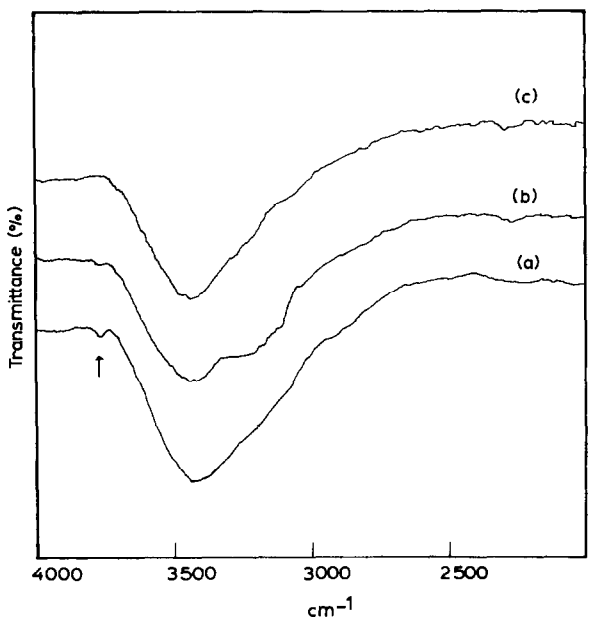

Fig. 2. IR spectra for catalyst samples 4 N (a); 3N (b) and 4N-500 (c).

attack a single Si–OH group to form another surface compound (B). However, no crystalline pattern is observed for this surface species. Also, one should not ignore the possibility that the nickel ammine complex might adsorb, by electrostatic attraction, on those sites which are unable to form a surface compound.

As the stability of Ni ammine complex is low [22] (compared, e.g., to Cu ammine complex) thermal treatment to 250°C destroys the crystalline surface silicate structure for all samples except that of 4N (15% NiO) through the evolution of ammonia. The stability of the crystalline structure of sample 4N-250 appears to result from the formation of this surface complex inside the pores. The high Ni concentration facilitates its penetration inside the pores and, upon thermal treatment to 250°C, the evolved ligands (molecular water from hydroxo ligand or ammonia) may remain in the vicinity of the solid matrix and, upon cooling, they are regained to satisfy the coordination of the nickel and form the surface complex again. As discussed below (next section) all ligands are evolved at temperatures $\lesssim$ 260°C.

Above 250°C, the surface silicate structure is destroyed and all samples from the different preparations are completely amorphous at 380°C.

At 500°C, all samples are amorphous except those from 3N and 4N, where two bands appear at *d*-distances of 2.201 and 2.049 ($2\theta = 48.0$ and 51.8, respectively) with the former peak the more intense (Fig. 3). One of these two bands, at a *d*-distance of 2.049, is close to the main band of the original preparations, which leads us to believe that these two bands may result from a surface complex of related nature. In the TG curve of hydrated $NiSO_4$ used in the present investigation 0.5 H_2O is found to remain attached to the salt after the dehydration of all other water molecules and is evolved in the temperature range 350–400°C (TG section). It thus appears that due to the relatively higher concentration of sulphate in samples 3N and 4N (Table 1, column 6), this amount of water is then significant as compared to that in samples 1N and 2N. Upon its evolution, the Ni present in either of the surface compounds, whether that attacking two silanol groups (compound A) or a single silanol (compound B), may take it to form an aquo ligand. But, as the amount of water evolved is small, if the surface compound (A) takes this water to give the observed pattern, it would have been expected to take place also at lower temperatures where small amounts of water are also evolved from the silica support. Whereas, for the amorphous surface compound (B) which originally possessed a hydroxo ligand and attacked a single hydroxyl group, the evolution of the ammonia and hydroxo ligands may produce a surface compound with unsaturated surface charges, and so, upon the evolution of water, being polar, is preferentially taken by this species to give the observed pattern. Thus a different *d*-spacing from that of the original surface silicate (A) is obtained.

At 1000°C, sample 4N shows two small broad bands characterising the presence of poorly crystalline NiO (Fig. 3). Sample 3N also exhibits these

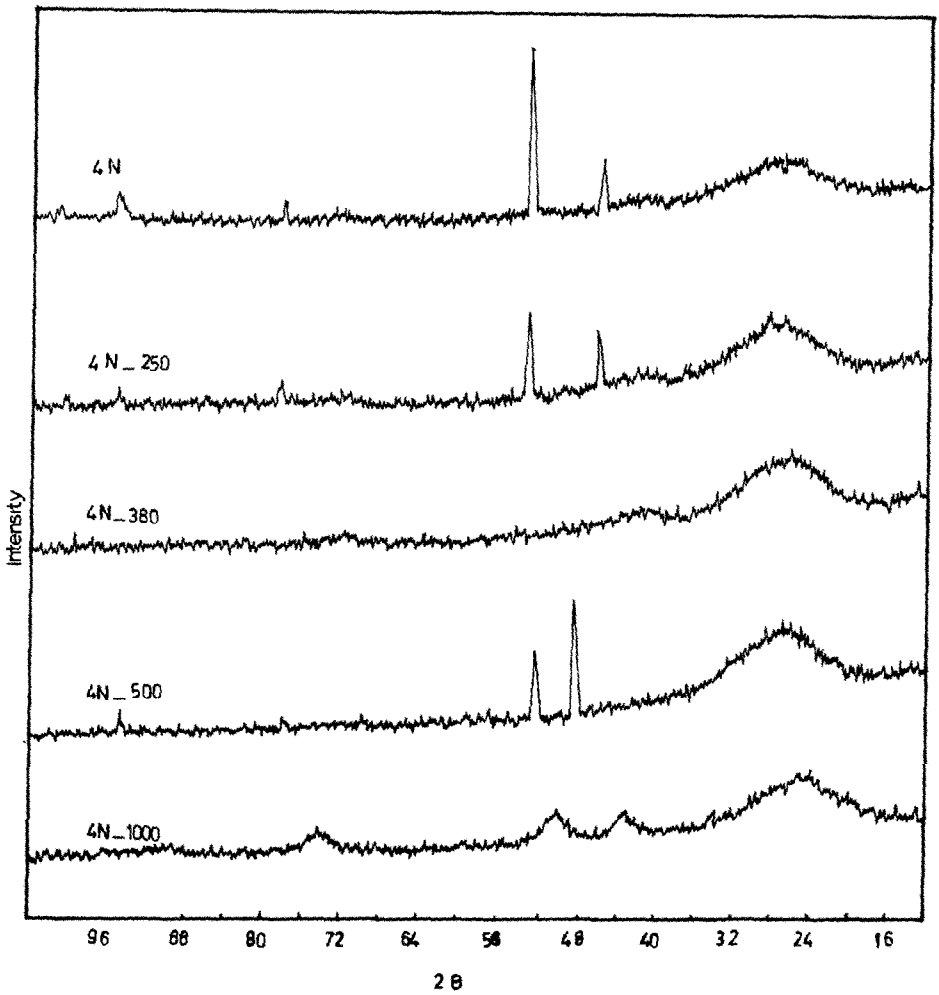

Fig. 3. X-ray diffraction patterns for catalyst 4N and its thermal decomposition products.

bands but to a much lower extent; the rest of the catalyst samples are amorphous.

The formation of crystalline (though poorly) NiO in samples 3N and 4N only may be suspected from the transformation to it of (1) the surface silicate (A), (2) the surface silicate (B) and (3) the presence of excess Ni ammine complex which was adsorbed by electrostatic forces only on the silica surface. The last two situations seem more likely to give rise to NiO, but the presence of a crystalline pattern from compound B in samples 4N-500 and to a lesser extent in 3N-500 leads us to believe that it is this compound which is responsible for the production of this highly distorted, poorly crystalline NiO, which is more pronounced for sample 4N than for sample 3N.

It is worth noting that all catalyst samples were black in colour at 1000°C, in spite of the amorphous nature of most of them.

Thermal analysis

The thermogravimetric curves of all the catalyst samples show an initial loss in weight which commences at temperatures $< 100°C$ and slows down at $\sim 200°C$. Figures 4 and 5 show the TG curves of the series 1N–4N, and samples $3N_b$ and $3N_c$, respectively. This loss in weight results from the evolution of physically adsorbed ammonia, ligand molecules (low stability of Ni ammine complex [22]) and H-bonded water which may either be attached to already adsorbed water molecules or to the surface hydroxyl groups. To evaluate the amount of evolved species, the intermediate linear region of the TG curves at temperatures 250–300°C is extrapolated backwards to intersect the extended line of the initial region of weight loss at 100–200°C, say at A (Fig. 4). This percentage weight loss is given in Table 1, column 3 which shows an increase in weight loss with increase in the Ni content. This is plausible since the presence of the ammonia (OH^- or H_2O) ligand will facilitate further adsorption of water molecules by H-bonding and the former is a function of the amount of nickel present.

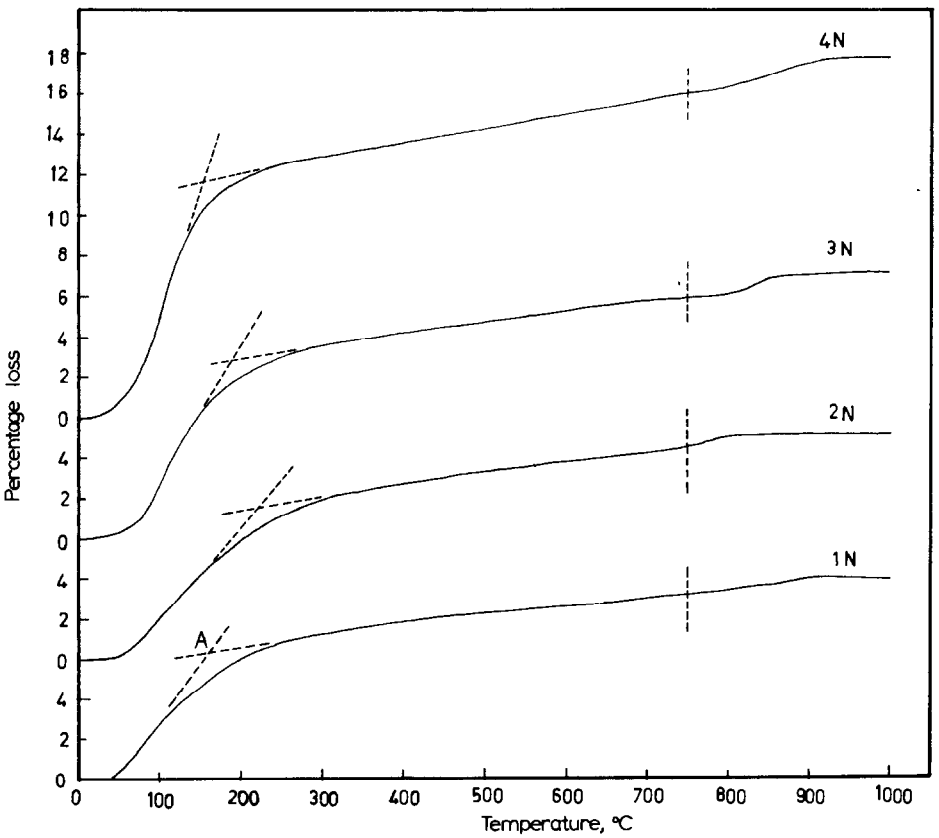

Fig. 4. Thermogravimetric curves for the catalyst series 1N–4N.

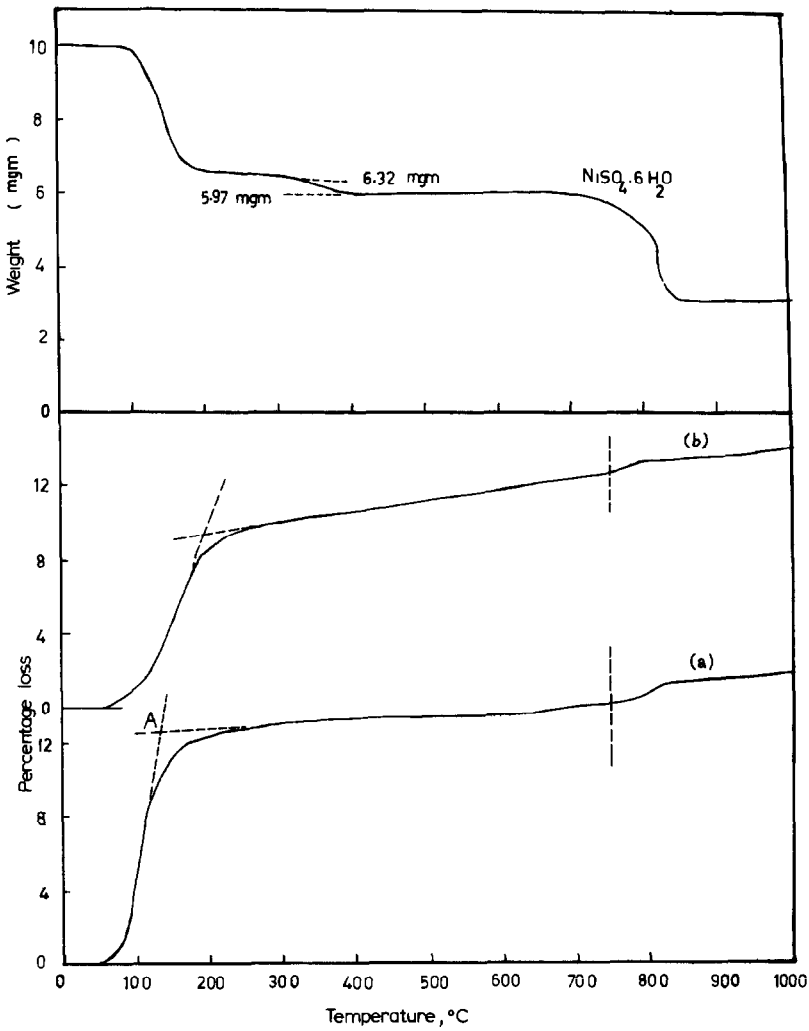

Fig. 5. Thermogravimetric curves for catalysts $3N_b$ (a); $3N_c$ (b) and $NiSO_4 \cdot 6H_2O$.

Following the intermediate linear region of weight loss, which arises from the evolution of the dehydroxylation of any unattacked silanol groups, any hydration water accompanying the Ni salt and any chemisorbed ammonia (Table 1, column 4), is a small but well defined step present at temperatures $> 750°C$. It characterizes the decomposition [23] of very small amounts of sulphate present, being detected by chemical analysis as well. An actual TG curve of $NiSO_4 \cdot 6H_2O$ used in this investigation showed that the sulphate decomposes at temperatures $> 750°C$ (Fig. 5). Thus, it is possible to estimate the amount of sulphate present from this stage of weight loss assuming any dehydroxylation to be negligible above 750°C. Analysis by thermogravimetry is found to be more efficient for small concentrations than

gravimetric methods of chemical analysis. The amounts of entrained SO_4^{2-} are given in Table 1, column 6. It is important to note that the TG curve of $NiSO_4 \cdot 6H_2O$ showed a small dehydration step in the temperature range 340–400°C corresponding to 0.5 H_2O—the experimental loss percentage is 5.53 (~ 5.5%) as compared to the theoretical loss percentage of 5.49 (~ 5.5%). This hydration water contributes to the weight loss of the intermediate temperature range.

DTA of all catalyst samples exhibit an endothermic peak centred at ~ 125°C for samples 1N, $3N_b$ and 4N whereas, samples 2N, 3N and $3N_c$ have this peak centered at 150–160°C. In all cases it corresponds to the first initial loss in the TG curves (Figs. 4 and 5). Another very small endotherm is observed for sample $3N_c$ and 4N only at ~ 275 and 260°C, respectively,

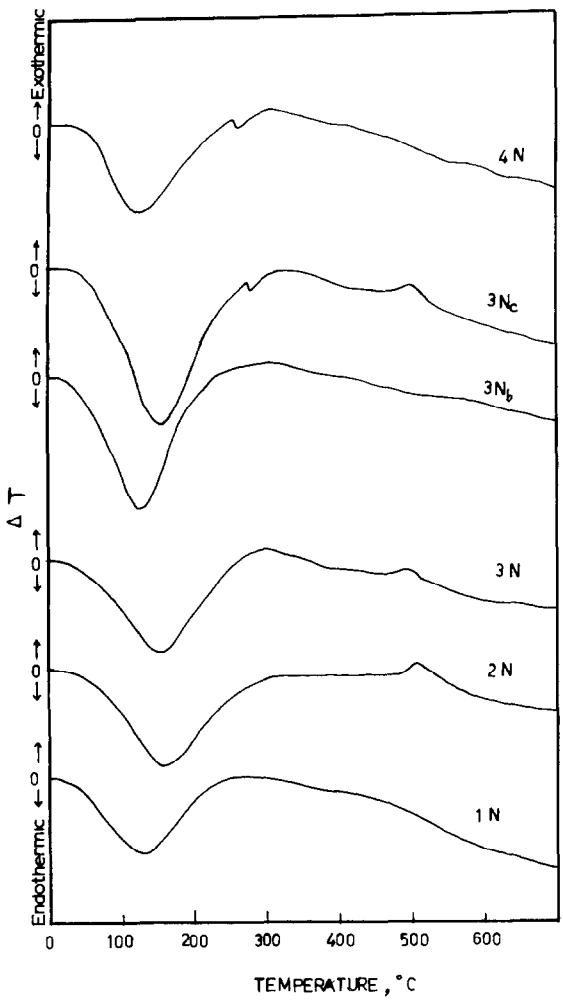

Fig. 6. Differential thermal analysis curves for catalyst samples 1N–4N, $3N_b$ and $3N_c$.

(Fig. 6). For the former sample this may arise from the evolution of chemisorbed ammonia which is probable considering the mode of its preparation, whereas for sample 4N, it results from the evolution of the hydroxo ligand. IR spectra of samples heated $> 250°C$ do not show the O–H vibration frequency at 1770 cm^{-1} observed for the original sample (Fig. 2, curve C).

At 500°C, a small broad exotherm is observed for samples 2N, 3N and $3N_c$ only. It may be interpreted as resulting from a partial auto-reduction process of nickel to a valency slightly below 2. This auto-reduction process has been observed in other oxide systems [24]. Nickel oxide is found to lose oxygen [16] upon thermal treatment in a limited supply of air, reaching the formula, e.g., $Ni_{24}O_{23}$ depending on the treatment temperature, but soon regains it upon exposure to air and exceeds the amount of oxygen necessary for the stoichiometry giving the oxide $NiO_{1.16}$ [25].

In the case of sample 4N, this small exothermic effect seems to be compensated by the endothermic evolution of the small amount of hydration water associated with the sulphate and which is evolved at a similar temperature range. It is important to recall that differences in the temperature as observed from TG and DTA data arise from the different transfer processes in the two techniques.

The amount of Ni in sample 1N is quite small and this exothermic effect is not detected, whereas for sample $3N_b$, the surface species could not be identified by the techniques employed, being amorphous to X-ray, and it may not undergo such a reduction process.

It is worth noting that the base line of the DTA curves is markedly shifted at higher temperatures and when the heating is conducted up to 700°C.

Surface area and pore structure

Effect of Ni concentration

Full nitrogen adsorption–desorption isotherms are obtained for catalyst preparations 1N–4N and their products after thermal treatment. All samples showed type II isotherms. Though sample 1N exhibited a closed hysteresis loop (closure pressure 0.40 P/P_0), increasing the Ni content to 5% produced a catalyst which gave rise to a completely reversible isotherm. Further increase to 10% (3N) and 15% (4N) gave rise to isotherms with small hysteresis loops with closure pressures of 0.40 and 0.25 P/P_0, respectively. All the thermal decomposition products produced closed hysteresis loops of varying sizes signifying the contribution of the Ni concentration in varying the pore structure of the resulting catalyst.

The specific surface areas were determined by the BET method in the conventional range of relative pressures. A value of 16.2 $Å^2$ is adopted for the molecular area of nitrogen.

To detect the existence of pores in the samples and to differentiate

TABLE 2

Surface characteristics of catalysts 1N, 2N and their thermally treated products

Catalyst samples	BET C-constant	S_{BET} ($m^2\ g^{-1}$)	S_t ($m^2\ g^{-1}$)	$V_{p_{0.95}}$ ($ml\ g^{-1}$)	r_H (Å)
1N	7	187.6	180.0	0.2464	13.13
1N-250	10	196.0	195.0	0.3388	17.28
1N-380	9	194.3	195.0	0.3203	16.48
1N-500	13	191.7	190.0	0.3449	17.98
1N-1000	12	181.4	185.0	0.2864	15.70
2N	8	125.8	125.0	0.1570	12.57
2N-250	6	120.8	120.0	0.1909	15.79
2N-380	8	146.1	145.0	0.2310	15.81
2N-500	6	123.7	120.5	0.2032	16.42
2N-1000	7	154.4	150.0	0.1925	12.47

between micro and mesopores, the t-method of de Boer [26] is applied. In these plots the t-curves of Mikhail et al. [27] (BET C-constant below 30) were employed which matched the corresponding BET C-constants of the samples under test and allowed for the correct estimate of S_t [28]. The agreement between S_t and S_{BET} is very good as observed for Tables 2 and 3 columns 4 and 3, respectively.

The specific surface area is found to decrease considerably upon increasing the Ni content from 2% to 5% which then increases only slightly for the 10% Ni content sample but markedly increases for that with 15% Ni content —the specific area is almost double that for sample 2N. These variations in area show that at NiO concentrations $\geqslant$ 10% there is either an additional or a different type of chemical attack of the support to that found in samples

TABLE 3

Surface characteristics of catalyst 3N and 4N and their thermally treated products

Catalyst sample	BET C-constant	S_{BET} ($m^2\ g^{-1}$)	S_t ($m^2\ g^{-1}$)	$V_{p_{0.95}}$ ($ml\ g^{-1}$)	r_H (Å)
3N	7	134.3	135.0	0.1724	12.93
3N-250	10	135.3	134.0	0.2620	19.37
3N-380	10	162.4	165.0	0.2479	15.26
3N-500	15	193.0	195.0	0.3110	16.11
3N-1000	10	163.6	165.0	0.2679	16.17
4N	10	244.5	245.0	0.2494	10.20
4N-250	17	215.4	215.0	0.2402	11.15
4N-380	36	302.3	305.0	0.3172	10.49
4N-500	39	282.6	280.0	0.3141	11.14
4N-1000	22	218.7	215.0	0.2648	12.17

with lower Ni concentrations. These may result from: (i) changes in the nature of the Ni ammine complex, e.g., different ligand as H_2O or OH^- or from a different coordination number for Ni, (ii) variations in the extent of penetration of the complex inside the support pore system and the consequent effects of the intensification of the fields of force in these pores [29] and (iii) increase in the tendency to imperfect disordered stacking upon increasing the nickel concentration. A high surface area for NiO/SiO_2 catalyst indicates a strong chemical attack of the support — the high specific area being derived from the high proportion of silicate [3]. Indeed, sample 4N contains the highest nickel concentration besides the presence of the Ni ammine complex with a hydroxo group (B) which may also be present, to a much lesser extent, in sample 3N. Thus, not only the adjacent silanol groups form a surface silicate but also a single silanol group is attacked. This is reflected on the increased BET C-constant of sample 4N (Table 3 column 2).

The total pore volume, $V_{p_{0.95}}$, taken as liquid volume at $P/P_0 = 0.95$, (Tables 2 and 3 columns 5) follows the same trend as the specific area upon increasing the Ni content. From data of average hydraulic pore radius, r_H, assuming parallel plate idealization (Tables 2 and 3 columns 6) a decrease is observed in pore sizes being marked for sample 4N. These variations may be interpreted by considering the effects produced by the Ni complex upon penetration into the pores of the support. Thus, for sample 1N the Ni complex seems to be mainly distributed on the external surface of the support and upon increasing the Ni content to 5%, it starts to attack the pores, blocking some of the narrower pores and attacking the walls of the wider ones giving rise to a smaller area, smaller volume and narrower pore radius. Upon increasing the Ni content to 10%, the penetration of the Ni complex takes place further into the pores and in doing so under the high tendency of the Ni complex to attack the surface (high concentration of Ni complex) rupturing of some of the internal constrictions occurs whereby new area and volume are exposed. The increased tendency to decondensation of silica at this high pH [30] and the long soaking period together with the increased Ni concentration all contribute to the widening of constrictions in the pores. Increasing the Ni content further, to 15%, where the hydroxo-ligand becomes of significance, a deeper penetration into the pore system is enhanced due to increased surface interaction.

This visualization of pore penetration and attack of the pore walls is reflected in the V_1–t plots of the samples. Thus, sample 1N shows some mesoporosity as indicated by the upward deviation at $t = 6$ Å which reverts back at $t = 12.2$ Å (Fig. 7). The slope of this upward deviation decreases upon increasing the Ni content and the V_1–t plot of sample 4N is found to be predominantly microporous (Fig. 8).

Thermal treatment at 250°C of catalyst 1N produces an increase in S_{BET}, $V_{p_{0.95}}$, and r_H. As this catalyst has a nickel content of 2%, the effect is mainly that arising from the silica carrier. The evolution of the dehydration water

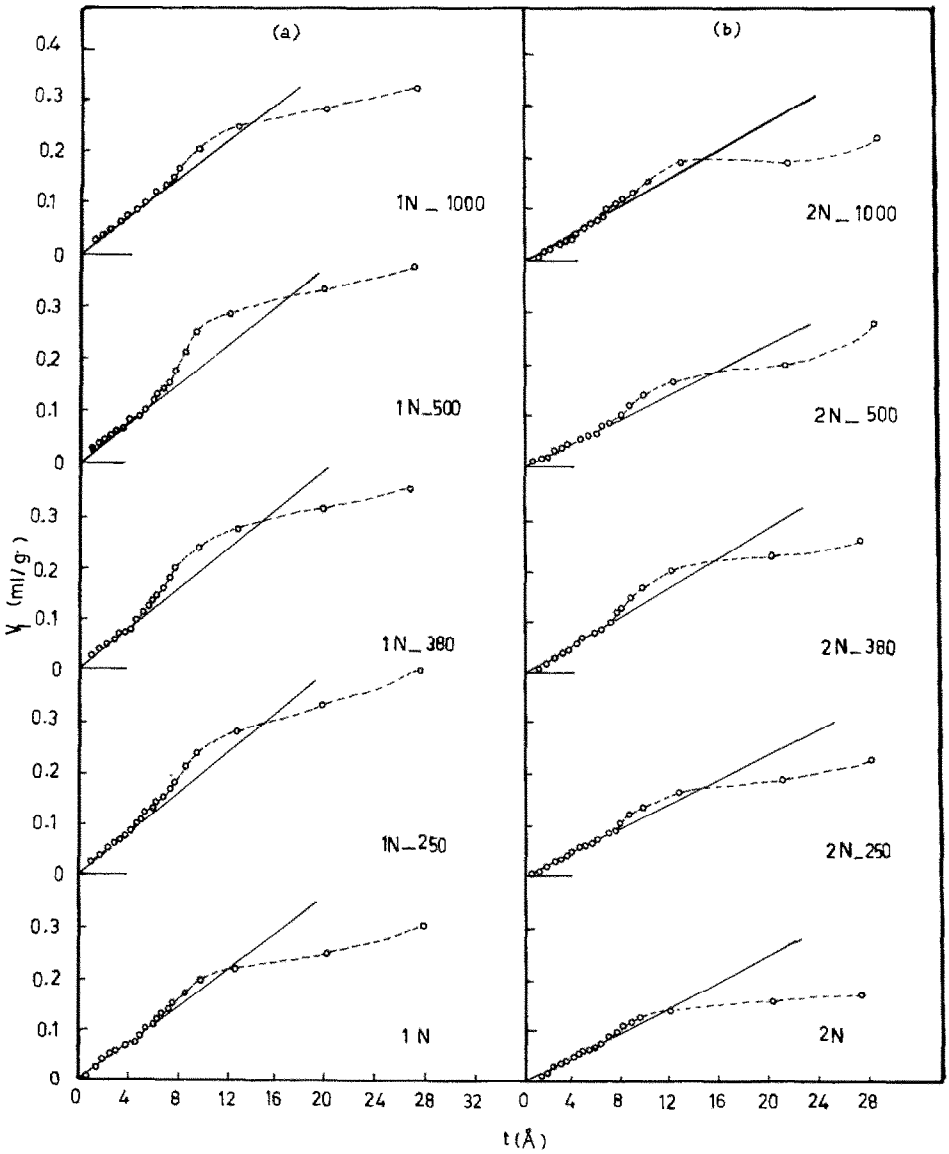

Fig. 7. V_1–t plots from N_2 adsorption on catalyst samples 1N (a) and 2N (b) and their products of thermal treatment.

and any adsorbed NH_3 species, and also the evolution of the ammonia ligand produce the observed changes which are accompanied by widening of the pores (Fig. 7). For catalyst samples 2N and 3N, the area changes only slightly at 250°C but a marked decrease is observed for sample 4N. The evolution of thermal products at this low temperature is usually followed by sintering, depending on the actual temperature investigated and on the nickel content, e.g., as in 4N-250 which seem to enhance this low tempera-

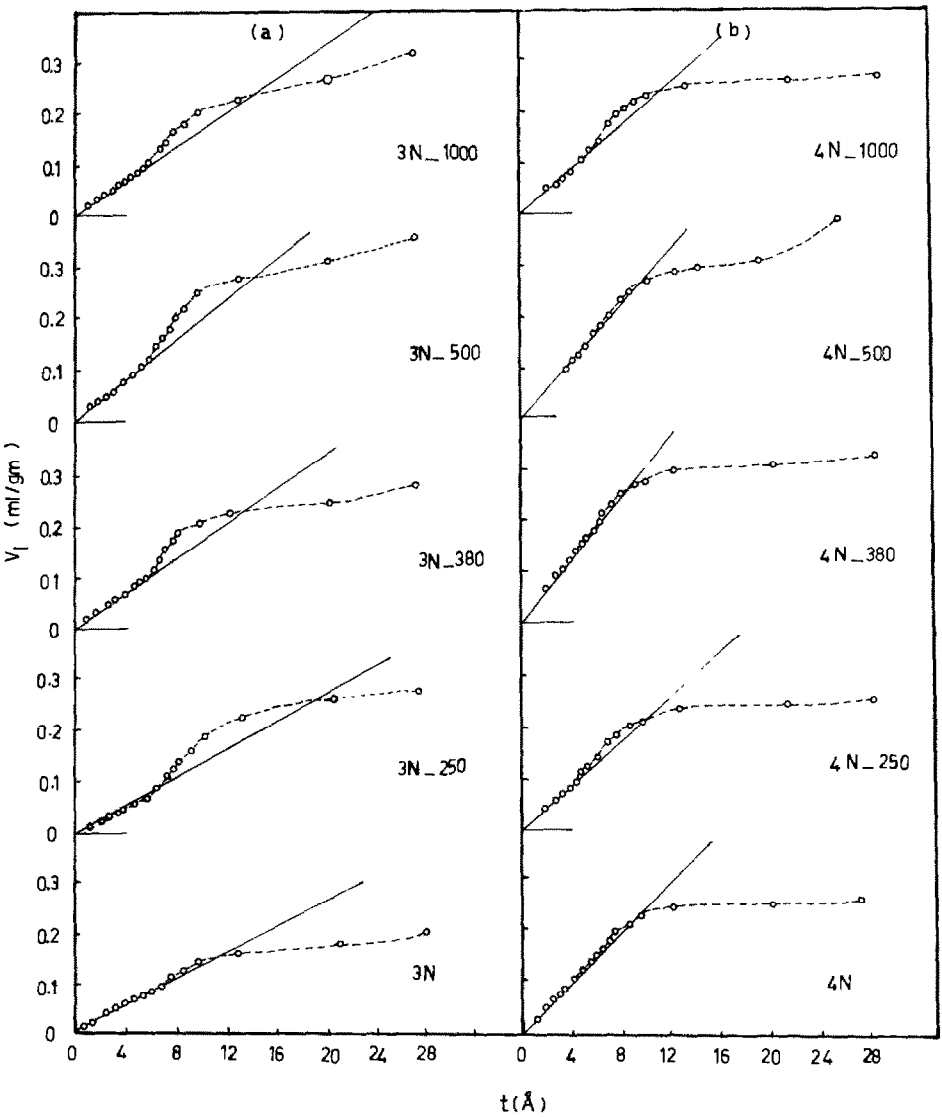

Fig. 8. V_1–t plots from N_2 adsorption on catalyst samples 3N (a) and 4N (b) and their products of thermal treatment.

ture sintering process [31]. Widening of the pores as a result of this agglomeration process is clearly observed in their V_1–t plots (Figs. 7 and 8). Sample 4N-250 shows the least increase in pore radius, probably due to the presence of increased nickel in the pores which may play a role in binding together, to a certain extent, the walls of the pore system.

An increase in area is observed at 380°C for all catalyst samples except 1N-380 which invariably remained the same. At this temperature range the water associated with the adsorbed sulphate (Fig. 5) is evolved and as catalyst 4N contains the largest Ni content, most of which is situated in the

pores, the evolution of this water will produce the observed effect which decreases with decrease in Ni content. The amount of water of hydration may differ from that of the salt $NiSO_4$ but is assumed to be comparable. However, the extent of penetration into the pores appears to be of significance in controlling the corresponding changes in total pore volume and average pore radii. Though an increase in total pore volume is observed for sample 2N-380 with relatively little change in the r_H value, sample 3N-380 shows a decrease in both $V_{p_{0.95}}$ and r_H, whereas sample 4N-380 possesses a much larger total pore volume with a slight narrowing of the pore radius showing the creation of new pores upon the water evolution which is large for sample 4N (Table 1, column 4). The changes in pore sizes for products from catalyst 3N and 4N are reflected in their corresponding V_1–t plots (Fig. 8). Thus, for 3N-380, the upward deviation commences at $t = 6$ Å and reverts back to cut the straight line passing through the origin at $t = 13.4$ Å as compared to sample 3N-250 which reverts back at $t = 18.8$ Å whereas for sample 4N-380, the upward deviation is very small and the sample is predominantly microporous with some mesopores (also reflected in the adsorption hysteresis loop). As the penetration of the nickel in catalyst 2N is not deep in the pores, the average pore radius is only slightly affected.

At 500°C, the effects produced by the evolution of water from the inner pores is still effective in producing high specific areas for samples 3N and 4N though the high specific area of sample 4N-380 partly masks this effect whereas for 1N and 2N sintering seems to commence.

At 1000°C the decomposition of the minute amounts of sulphate is expected to bring about an increase in area [32] if its effect counterbalances the sintering process which is enhanced by the nickel present. This is observed for sample 2N only but for the rest of the samples a decrease in specific area is obtained.

Narrowing of the pores is observed at this temperature for catalysts 1N–3N whereas for catalyst 4N widening is observed from their corresponding V_1–t plots (Figs. 7 and 8). Thus, all thermally treated products of catalysts series 1–3N are composed of a mixed pore system containing both meso and micropores, whereas samples from 4N are predominantly microporous, mesoporosity increasing only by thermal treatment at 250 and 1000°C.

It should be noted that catalyst 4N possesses the highest areas at all temperatures investigated.

Role of method of preparation

N_2 adsorption–desorption cycles are obtained for samples $3N_b$ and $3N_c$ which contain nearly the same Ni-content as sample 3N (Table 1 column 2) but prepared under different experimental conditions. The isotherms of these catalyst samples and their thermally treated products are type II and exhibit

TABLE 4

Surface characteristics of catalyst $3N_b$ and $3N_c$ and their thermally treated products

Catalyst sample	BET C-constant	S_{BET} ($m^2\ g^{-1}$)	S_t ($m^2\ g^{-1}$)	$V_{P_{0.95}}$ ($ml\ g^{-1}$)	r_H (Å)
$3N_b$	9	113.9	115.0	0.1478	12.97
$3N_b$-250	10	108.9	120.0	0.2618	24.04
$3N_b$-380	9	150.71	148.0	0.2772	18.39
$3N_b$-500	8	118.5	125.0	0.2541	21.44
$3N_b$-1000	12	150.0	158.0	0.3388	22.58
$3N_c$	5	159.5	154.0	0.2464	15.44
$3N_c$-250	6	130.3	130.0	0.2002	15.36
$3N_c$-380	8	111.0	115.0	0.1909	17.19
$3N_c$-500	7	124.7	120.0	0.1878	15.05
$3N_c$-1000	10	117.6	115.0	0.1848	15.78

closed hysteresis loops of varying sizes. Table 4 shows their specific surface areas, S_{BET} and S_t, as well as the BET C-constants (columns 3, 4 and 2, respectively).

The surface area of sample $3N_b$ and all its heated products are lower than the corresponding samples from 3N. Its variation with temperature is similar to that of 2N and not 3N showing a maximum at 380°C and an increase at 1000°C. This increase at 1000°C is not unexpected but is found in other sulphate-containing oxide systems being accompanied by an increase in total pore volume [32]. The amorphous nature of this catalyst emphasizes either the complete absence of the surface silicate structure or its formation in crystallite sizes < 50 Å. However, the increase in area at 1000°C may indicate the presence of an actual amorphous nickel oxide-sulphate which is favoured by drying at room temperature. Its presence may exist in the other catalyst preparations but to a much lower extent and, therefore, its effect on the specific area and total pore volume may be negligible.

As the only difference between this sample and 3N is the drying temperature, it appears that in spite of the high nickel concentration ($\sim 10\%$ NiO) the nickel did not penetrate enough into the pores but remained attached to the surface and/or just at the entrances of these pores. This is reflected on the larger values of average pore radius of the thermal products (Table 4, column 6).

The corresponding V_1–t plots show the absence of microporosity for the heated products (Fig. 9). The upward deviation commences at a t-value of 6.2 Å for heat treatment at 250°C, but as some pores of smaller dimensions appear upon heating to 380°C an increase in area and decrease in r_H values result with a corresponding appearance in the V_1–t plot of a new group of pores starting at a t-value of 5 Å accompanied by a decrease in the slope of the further upward deviation at $t = 6$ Å. As to the original catalyst $3N_b$, its

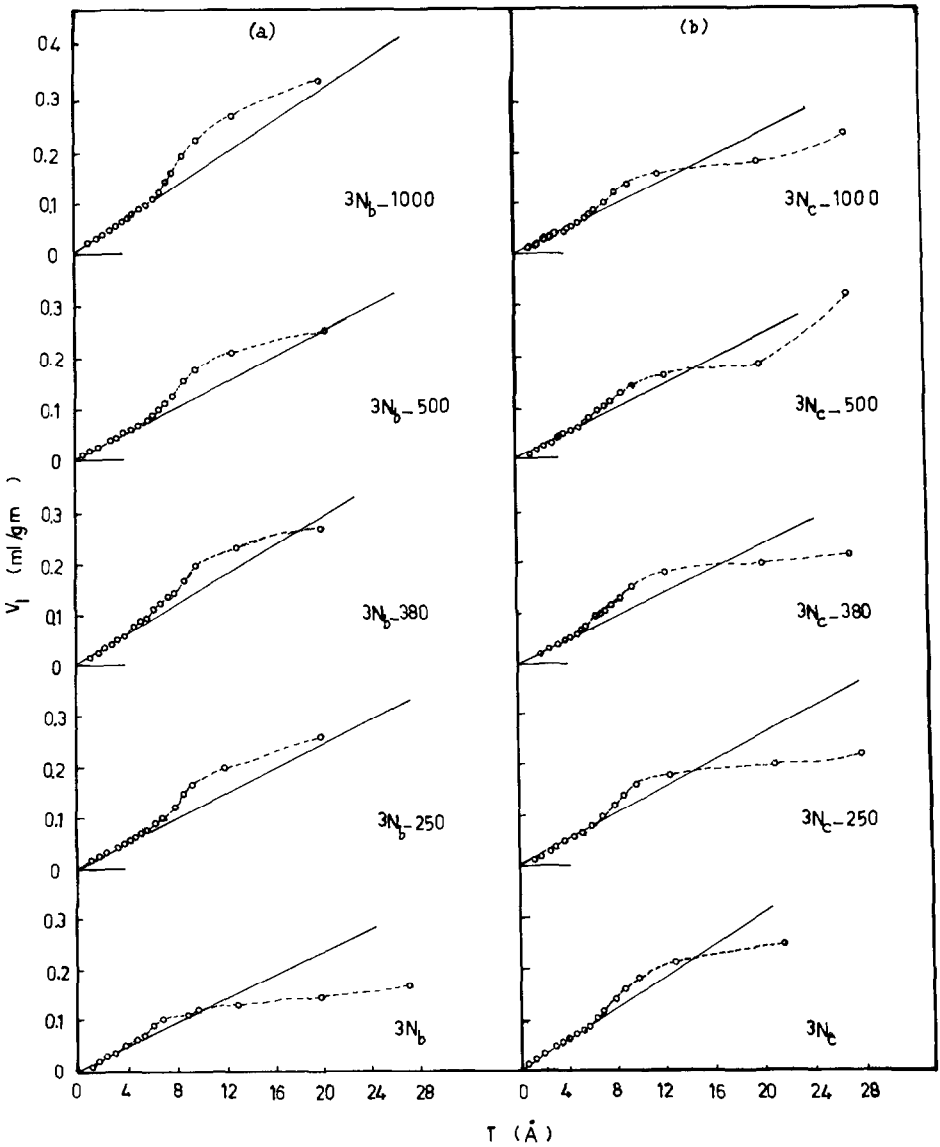

Fig. 9. $V_l - t$ plots from N_2 adsorption on catalyst samples $3N_b$ (a) and $3N_c$ (b) and their products of thermal treatment.

$V_{P_{0.95}}$ and r_H values are comparable with those of 2N as well as the presence of microporosity is clear from Fig. 9(a).

Thus, the significance of heat treatment at 80°C for a long period (~ 12 h) lies in supplying the required energy (i) to form a crystalline surface silicate and (ii) to overcome the increased field of force in the pores and facilitate penetration through the energy barrier at any constrictions which may hinder their passage at ordinary temperatures.

As to sample $3N_c$, though it possesses a higher area, all its thermally treated products have specific areas which are lower than those of 3N. A continuous decrease is observed up to 380°C, followed by a small increase at 500°C which seems to result from the evolution of the little hydration water associated with the adsorbed sulphate. A continuous decrease in total pore volume with thermal treatment is also observed although the changes in the temperature range 250–1000°C are quite small (Table 4, column 5). The V_1–t plots of the original and thermally treated samples show them to be composed of a mixed pore system–mesopores co-existing with micropores (Fig. 9(b)).

The variations in surface parameters for sample $3N_c$ are different from those of 3N, though the percentage losses at the different stages are comparable to it (Table 1), which brings the belief that the surface species may be different. Since the $NiSO_4$ attacks first the surface, the addition of ammonia solution later may either form the ammine complex with the adsorbed nickel and/or attack a bare SiO_2 surface. A study of the effect of ammonia alone on mesoporous and microporous silica gel is given elsewhere [33]. What actually takes place is not clear, yet the absence of the crystalline species for the surface silicate previously observed for sample 3N is evident from the amorphous nature noted from its XRD pattern, though crystallite sizes < 50 Å may have formed on the surface.

REFERENCES

1 S.R. Morrison, The Chemical Physics of Surfaces, Plenum Press, New York, 1977.
2 J. Cosyns, M.T. Chenebaux, J.F. Le Page and R. Montarnal, in B. Delmon, P.A. Jacobs and G. Poncelet (Eds.), Preparation of Catalysts, Elsevier, Amsterdam, 1976.
3 J.W.E. Coenen and B.G. Linsen, in B.G. Linsen (Ed.), Physical and Chemical Aspects of Adsorbents and Catalysts, Academic Press, New York, 1970.
4 J. Cervello, E. Hermana, J.F. Jiménez and F. Melo, in B. Delmon, P.A. Jacobs and G. Poncelet (Eds.), Preparation of Catalysts, Elsevier, Amsterdam, 1976.
5 M. Houalla, Stud. Surf. Sci. Catal. 16 (Prep. Catal. 3), (1983) 273.
6 T. Hidemitsu, Y. Ono and T. Keii, J. Catal., 40 (2) (1975) 197.
7 R.L. Burwell, Jr., R.G. Pearson, G.L. Haller, P.B. Tjok and S.P. Chok, Inorg. Chem., 4 (1965) 1123.
8 A.A. Danisov and B.A. Zhidkov, Katal. Katal., 9 (1972) 103.
9 G. Rienäcker, Abh. Dtsch. Akad. Wiss. Berlin, Kl. Chem. Geol. Biol., 3 (1956) 8.
10 H. Taylor, Adv. Catal., 9 (1957) 1.
11 P. Desai and J.T. Richardson, in B. Delmon and G.F. Froment (Eds.), Catalyst Deactivation, Elsevier, Amsterdam, 1980.
12 J. Bagg, H. Jaeger and J.V. Sanders, J. Catal., 2 (1963) 449.
13 J. Uhara, T. Hikino, Y. Numata, H. Hamada and Y. Kageyama, J. Phys. Chem., 66 (1962) 1374.
14 R.B. Shalvoy, P.J. Rencroft and B.H. Davis, IMMR 46-PD 22-80, Surf. Struct. Mech. Gasie (Catal. Deactivation), 1980, pp. 14–23.
15 G. Wendt, H. Siegel and W. Schmitz, Cryst. Res. Technol., 17 (11) (1980) 1435.

16 B.S. Girgis, M.E. Mourad and T.M. Ghazi, Surf. Technol., 7 (1978) 367.
17 Suzy A. Selim, Said Hanafi, Mohamed Abdel-Khalik and Mohamed Ismail, J. Chem. Technol. Biotechnol., in press.
18 J.V. Smith, (Ed.), X-ray Powder Data File and Index To X-ray Data File, A.S.T.M., Philadelphia, PA, 1961.
19 Powder Diffraction File, A.S.T.M. Alphabetical Index of Inorganic compounds Published by the International center for diffraction data, Swathmore, PA, 1978.
20 Suzy A. Selim, Hamdy A. Hassan, M. Abd-El Khalik, and Raouf Sh. Mikhail, Thermochim. Acta, 45 (1981) 349.
21 J.P. Brunelle, Pure Appl. Chem., 50 (1978) 9.
22 Lars Gunnar Sillén, in Stability Constants of Metal-ion Complexes, Spec. Publ. No. 17, The Chemical Society, London, 1964.
23 C. Duval, Inorganic Thermogravimetric Analysis, Elsevier, Amsterdam, 1963.
24 A. Amin, Berlant A. Khalifa, and Suzy A. Selim, Surf. Technol., 21 (1984) 73.
25 S.A. Hassan, S.A. Selim, M.M. Mekawi and S. Hanafi, Appl. Catal., submitted.
26 B.C. Lippens, B.G. Linsen and J.H. deBoer, J. Catal., 3 (1964) 32; B.G. Linsen and J.H. deBoer, J. Catal., 4 (1965) 3, 9.
27 R.Sh. Mikhail, N.M. Guindy and S. Hanafi, Egypt J. Chem. Spec. Issue, Tourky, (1973) 53.
28 R.Sh. Mikhail and F. Shebl, J. Colloid Interface Sci., 34 (1) (1970) 65.
29 S.J. Gegg and K.S.W. Sing, Adsorption, Surface Area and Porosity, Academic Press, New York, 1967.
30 C. Okkerse, in B.G. Linsen (Ed.), Physical and Chemical Aspects of Adsorbents and Catalysts, Academic Press, New York, 1970.
31 R.Sh. Mikhail and S.A. Selim, J. Appl. Chem. Biotechnol., 24, (1974) 557.
32 Suzy A. Selim, Anwar Amin and Paul G. Rouxhet, Thermochim. Acta, 58 (1982) 211.
33 Suzy A. Selim, Hamdy A. Hassan, M. Abd-El-Khalik, and Raouf Sh. Mikhail, Surf. Technol., 14 (1981) 359.